J Solid State Electrochem (2012) 16:3449–3456
DOI 10.1007/s10008-012-1766-8

ORIGINAL PAPER

Pattern formation during electrodeposition of indium–cobalt alloys

I. Krastev · Ts. Dobrovolska · U. Lačnjevac · S. Nineva

Received: 21 March 2012 / Revised: 27 April 2012 / Accepted: 30 April 2012 / Published online: 15 May 2012
© Springer-Verlag 2012

Abstract The investigations on the effect of the electrolysis conditions, including high speed electroplating, on the content, structure, morphology and some properties of electrodeposited In-Co alloys from citrate electrolytes are presented. It was shown that indium and cobalt could be successfully deposited from acid citrate electrolytes and deposition of alloys with indium content between 20 and 80 wt. % is possible. At high cobalt content, heterogeneous multiphase coatings with spatio-temporal structures are obtained. Spatio-temporal structures could be observed also during electrodeposition under intensive hydrodynamic flow and improved mass transport conditions at high current densities. The structures are obtained for the first time from silver- and cyanide-free non-alkaline stable electrolytes of a relatively simple composition.

Introduction

Some investigations on the electrode processes, the physicochemical characteristics of deposited Ag-In alloy coatings and the pattern formation on their surface during electrodeposition were reported some years ago [1]. Recently some results concerning the electrolytic deposition of silver–cobalt alloys were published [2, 3]. In all these studies, the electrodeposition of silver-based alloys was described. Usually cyanide electrolytes are used for silver deposition, i.e. the silver ions are bonded in strong complexes. In order to bring the potentials of both metals close to each other some other complex forming agents are used which results in a complicated composition of the alloy electrolytes [4–9]. Recently it has been established that during electrodeposition of In-Co alloys pattern formation could also be observed [10]. In this case, we observed for the first time self-organization phenomena during electrodeposition of an alloy system in absence of silver. The spatio-temporal structure formation in the indium–cobalt system offers new possibilities for investigation of the self-organization phenomena during alloy electrodeposition from an electrolyte with simple composition.

Recently, the strong effect of addition of small indium amounts to some well-known and thoroughly studied permanent magnet materials like some cobalt alloys was reported [11]. The decrease of the sintering temperature and the high values of coercivity which could be reached without loosing the magnet density have been associated with the indium-rich grain-boundary phases. High values of coercivity were also registered during our preliminary investigations on the magnetic properties of electrodeposited indium–cobalt alloys.

The electrodeposition of In-Co alloy coatings has not been extensively studied and there is only one known paper in the literature regarding this topic. Sadana et al. [12] investigated the effect of the current density on the current efficiency and the composition of Co-In coatings electrodeposited from aqueous solutions. Despite of the extensive studies, the data about the electrode processes and the morphology of the deposits reported by Sadana and coworkers are very limited.

The present work was aimed at the investigations on the effect of the electrolysis conditions, including high speed electroplating, on the content, the structure, morphology and some properties of electrodeposited In-Co alloys from citrate electrolytes.

I. Krastev · T. Dobrovolska (✉) · S. Nineva
Institute of Physical Chemistry, Bulgarian Academy of Science,
1113 Sofia, Bulgaria
e-mail: tsvetina@ipc.bas.bg

U. Lačnjevac
Institute for Multidisciplinary Research,
11030 Belgrade, P.O. Box 33, Serbia

Experimental

The compositions of the investigated electrolytes are given in Table 1.

Electrolytes 1–4 were used only for cyclic voltammetry investigations. Electrolytes A, B and C were used for deposition of alloy coatings. The pH value of the used electrolytes was between 3.1 and 3.3. The electrolytes were prepared using chemicals of *pro analisi* purity and distilled water.

The cyclic voltammetry experiments were performed in a 100 cm^3 tri-electrode glass cell at room temperature. Platinum working electrode (area 1 cm^2) was used. The two counter electrodes were made from platinum. An Ag/AgCl reference electrode ($E_{Ag/AgCl}$=0.197 V vs. SHE) was used.

The experiments were performed at room temperature by means of a computerized potentiostat/galvanostat Princeton Applied Research Model 273 using the software Soft Corr II. The alloy coatings with thickness between 3 and 10 μm were deposited onto brass or copper cathodes with dimensions of 2×1 cm in the glass cell. The preliminary preparation of the cathodes includes a standard procedure of electrochemical degreasing followed by pickling in a 20 % solution of sulphuric acid. Two Pt/Ti counter mesh electrodes were used.

The In percentage in the coatings depending on the electrodeposition conditions was determined by X-ray fluorescence analysis (Fischerscope XDAL). The thickness and the percentage of the coatings were measured in 9 positions in the upper, middle and lower part of the electrode (3 measurements in each height).

The In or Co distribution on the surface of the coatings was examined by energy dispersive X-ray analysis (EDX) and the morphology of the coatings surface was investigated by scanning electron microscopy (SEM).

X-ray diffraction patterns for phase identification of the deposited alloy coatings were recorded in the interval 20–120° (2Θ) with a Philips PW 1050 diffractometer with $Fe_{K\alpha}$-irradiation and scintillation detector.

The internal stress, *IS*, was monitored with the apparatus constructed by Stalzer [13] operating on the principle of the one-sided galvanized bendable cathode. The copper cathodes were 7 cm long, 1 cm wide, 0.3 mm thick and their backsides were lacquer-insulated. During electrodeposition, the cathode is bending in a specific direction depending on whether the induced internal stress is compressive or tensile. A sensor detects the deviation and compensates it through an electric feedback system. The force needed for compensation and hence the value of the internal stress is deduced from the electrical signal. The latter is transferred through a suitable interface to a computer for monitoring and processing. The method permits in situ monitoring of the internal stress during electrodeposition.

The Jet-plating process was realized in a special experimental device (Jet-lab). The construction of the cell is described elsewhere [14]. The cathodes were brass sheets with a surface of 2.2×3.3 cm^{-2} and the localized area for the deposition was 1.77 cm^{-2}. The coatings with a thickness of about 1–2 μm were deposited at room temperature at the flow speed of the electrolyte of 600 $dm^3\ h^{-1}$. The electrolyte was injected into the electrolyte cell through a titanium nozzle, connected as anode.

The constants, used for the calculation of the possible species in the investigated electrolytes, are presented in the Table 2 [15]. The calculation of the species distributions was performed by using the program *Hyperquad simulation and speciation* (*HySS*) [16].

Results and discussion

The difference between the standard electrode potentials of indium and cobalt ($E^0_{(Co^{2+}/Co)}$=−0.277 V [17], $E^0_{(In^{3+}/In)}$= −0.34 V [18]) is not very large and co-deposition of both metals could be obtained without using any strong complexing agents. In spite of this, in order to obtain coatings of good quality, electrolytes containing complex compounds like citrate and tartrate have been used in this study (Table 1).

Different species could exist in the investigated electrolytes for alloy deposition depending on the pH range. It has been specified in several papers [19–22] that there are no available data on indium citrate complexes. The available data in Table 2 exclude the probability of formation of

Table 1 Electrolyte composition

Electrolyte no.	In as $InCl_3$ g dm^{-3}/M	Co as $CoSO_4 \cdot 7\ H_2O$ H_2O g dm^{-3}/M	$(NH_4)_2$HCitrate g dm^{-3}/M	KNaTartrate g dm^{-3}/M
1	5/0.044	–	–	–
2	5/0.044	–	20/0.09	–
3	–	30/0.5	–	–
4	–	30/0.5	20/0.09	–
A	5/0.044	30/0.5	20/0.09	–
B	5/0.044	30/0.5	40/0.18	–
C	5/0.044	30/0.5	40/0.18	5/0.024

Table 2 Constants used for the calculation of the species distribution

No.	Reactions	log β
1.	$Cit^{3-} + H^+ \leftrightarrows HCit^{2-}$	6.4
2.	$Cit^{3-} + 2H^+ \leftrightarrows H_2Cit^-$	11.16
3.	$Cit^{3-} + 3H^+ \leftrightarrows H_3Cit$	14.29
4.	$Co^{2+} + HCit^{2-} \leftrightarrows CoHCit$	4.8
5.	$Co^{2+} + Cit^{3-} \leftrightarrows CoCit^-$	12.5
6.	$Co^{2+} + Tar^{2-} \leftrightarrows CoTar$	2.1
7.	$Tar^{2-} + H^+ \leftrightarrows HTar^-$	4.37
8.	$Tar^{2-} + 2\ H^+ \leftrightarrows H_2Tar$	7.4
9.	$In^{3+} + H_2O \leftrightarrows InOH^{2+} + H^+$	−3.54
10.	$In^{3+} + 2H_2O \leftrightarrows In(OH)_2^+ + 2\ H^+$	−7.82
11.	$In(OH)_3(s) \leftrightarrows In^{3+} + 3OH^-$	−33.9
12.	$In^{3+} + Cl^- \leftrightarrows InCl^{2+}$	1.42
13.	$In^{3+} + 2Cl^- \leftrightarrows InCl_2^+$	2.23
14.	$In^{3+} + 3Cl^- \leftrightarrows InCl_3$	3.23
15.	$In^{3+} + Cit^{3-} \leftrightarrows InCit$	6.18
16.	$In^{3+} + Tar^{2-} \leftrightarrows InTar^+$	4.44
17.	$In^{3+} + 2Tar^{2-} \leftrightarrows InTar_2^-$	8.46

strong complexes of In^{3+} with citrate anions. If such a complex formation is possible, the stability constants of the formed complexes should be very small and therefore their presence in the solution should be neglected. The possibility of formation of $In(NH_4)x$ complexes could be ruled out in the investigated pH range. The $In(OH)_3(s)$ precipitation commences at a pH value of approximately 3.5, which sets the upper pH limit of the electrolytes for indium deposition.

The formation of $Co(OH)_2(s)$, $[CoOH^+]$ and $[Co(NH_3)x]$ species, since they all exist only in basic media, is irrelevant for calculations at pH less than 8. Figure 1a,b show the possible existence at different pH values of the species in the electrolyte A, B and C, calculated by the HYSS programme [16].

In the citrate containing electrolyte A, cobalt forms two complexes, $CoCit^-$ and CoHCit, (<< 0.05 M) but since the former one is much more stable, it dominates in the solution. In the electrolyte B, where the concentration of di-ammonium hydrogen citrate is already 0.18 M, the possible complexes are also $CoCit^-$ and CoHCit, but the relative quantity of the $CoCit^-$ would be about 0.18 M. In the electrolyte C, after addition of potassium-sodium tartrate, according to HYSS calculation (Fig. 1b), about 0.01 M of In ions is organized in a $InTar^+$ complex and almost the same amount is bonded in the $InTar_2^-$ complex. It could be expected that the addition of potassium sodium tartrate will favour the cobalt electrodeposition due to the bonding of a part of indium ions in tartrate complexes.

The formation of different complexes in the investigated electrolytes in the presence of tartrate and citrate ions results

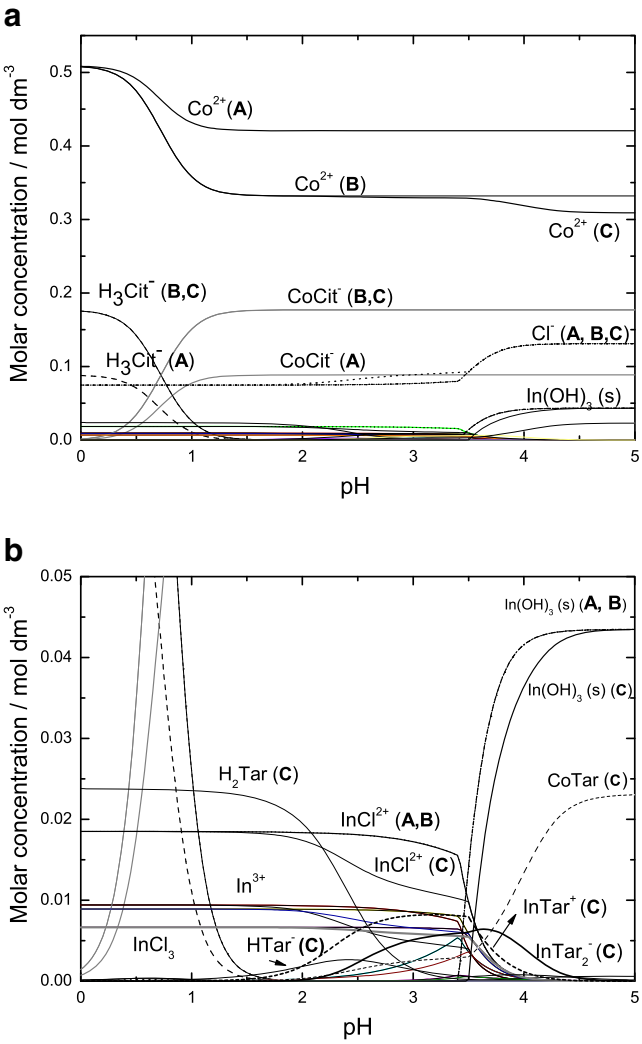

Fig. 1 **a** Possible distribution of the species in the electrolyte *A*, *B* and *C* calculated by HYSS system. **b** Fig.1a in the range of molar concentration 0–0.05 M

in changes in the deposition potentials of both metals compared to the deposition from simple electrolytes, which could be detected by cyclic voltammetric investigations.

Figure 2 shows the cathodic parts of the cyclic voltammograms recorded in the investigated electrolytes (Table 2). Curves 1 and 3 present the deposition of the pure metals from their simple aqueous solutions. The difference in the reduction potentials of both metals is negligible. In the presence of di-ammonium hydrogen citrate (curves 2 and 4) the electrochemical reactions start at more positive potentials (around −0.35 V). The difference between the deposition potentials of both metals is again negligible.

The deposition starts in electrolytes A, B and C at potentials around −0.35 V. The cathodic curves run at low potentials similar to the curve of indium deposition and at higher potentials (around −1.0 V) the current increases similar to the case of cobalt deposition. The increase of the citrate

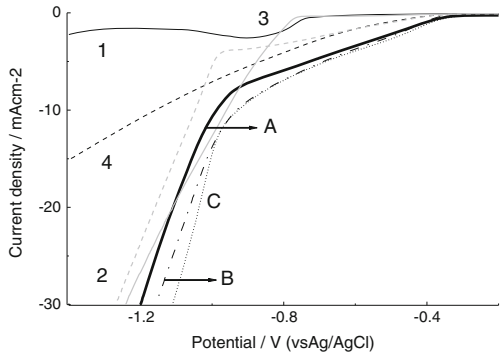

Fig. 2 Cathodic parts of the cyclic voltammetric curves for the investigated electrolytes, onto Pt electrode, scan rate 25 mV s^{-1} (*lines*, corresponding to electrolyte *1 solid black*, electrolyte *2 dashed black*, electrolyte *3 solid grey*, electrolyte *4 dashed grey*, electrolyte *A thick black*, electrolyte *B dash dot black*, electrolyte *C dotted black*

concentration (electrolyte B) leads to an increase in the rate of the electrochemical reaction facilitating the hydrogen evolution reaction. The addition of tartrate ions to electrolyte B (electrolyte C) does not result in any significant changes in the deposition curve. The possible differences in the deposition rates of both metals during the alloy deposition should be a result of the accompanying hydrogen evolution reaction.

Figure 3 shows the relationship between the indium content in the alloy and the current density. Indium deposits preferentially in all three electrolytes and the tartrate ions inhibit the indium deposition, so that indium poorer coatings are deposited from electrolyte C compared to the coatings from electrolyte B. These results correspond very well to the results from the calculation of the possible distribution of the species by HYSS (Fig. 1) as well to the cyclic voltammetry investigations (Fig. 2).

At low current densities (up to 0.5 Adm^{-2}), the coatings are light–grey and matt. This appearance corresponds to a content of indium of about 70 wt. %. The increased current density leads to more recognizable heterogeneity of the surface of the deposits. Coatings with indium content of 60–30 wt. % could be obtained from the three investigated electrolytes in the range of 0.6–1.2 A dm^{-2}. The deposition

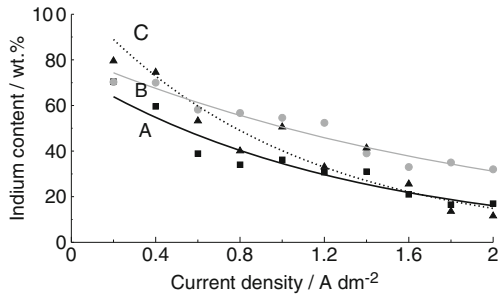

Fig. 3 Indium content in the obtained coatings in dependence on the current density in the electrolytes: *A filled square*, *B filled circle*, *C filled triangle*

rate of the alloy coatings is between 0.05 and 0.15 μm min^{-1} depending on the applied current density. When the content of indium is in the range between 50 and 30 wt. %, different areas of the electrode surface are covered by spatio-temporal structures in form of targets, waves and spirals. This content could be reached at current densities between 0.9–1.2 A dm^{-2}. The optical image of a part of the electrode, covered by the structures is shown in Fig. 4. The patterns could be observed in all investigated electrolytes (A, B and C), with a small differences in the applied current densities.

Scanning electron microscopy images of a similar coating with different magnifications are shown in Fig. 5a–c. The morphology of the different zones is different due to the phase heterogeneity of the deposits. The EDX analysis shows that the indium contents in the different dark and light zones differ not so much and vary between 38 and 32 wt. %. The light areas in the BEC images are finer grained than the dark ones (Fig. 5c). Most possibly, the wave fronts move with a sufficiently high speed during deposition, so that the thickness of the formed dark and light layers during deposition is substantially smaller than the penetration depth of the electron-beam during EDX analysis. As a result the beam penetrates through several light and dark layers, and the estimated average content of indium in both zones is similar.

The XRD spectra of the coatings, deposited in the electrolyte A at different current densities, are presented in Fig. 6. The spectra were recorded in the 2Θ interval between 20 and 120°, but for better visualization the record is presented in the interval 35–75°. The reflexes of In (PDF 03-065-9292, tetragonal, with cell parameters a=3.253 Å, b=4.9455 Å) and of the phases $CoIn_3$ (PDF 03-65-5582, tetragonal, with cell parameters a=6.829 Å and c=3.547 Å) are detected in the all obtained spectra.

Fig. 4 Optical image of a coating, obtained at current density 1.2 A dm^{-2} from the electrolyte *B*, time of deposition—30 min

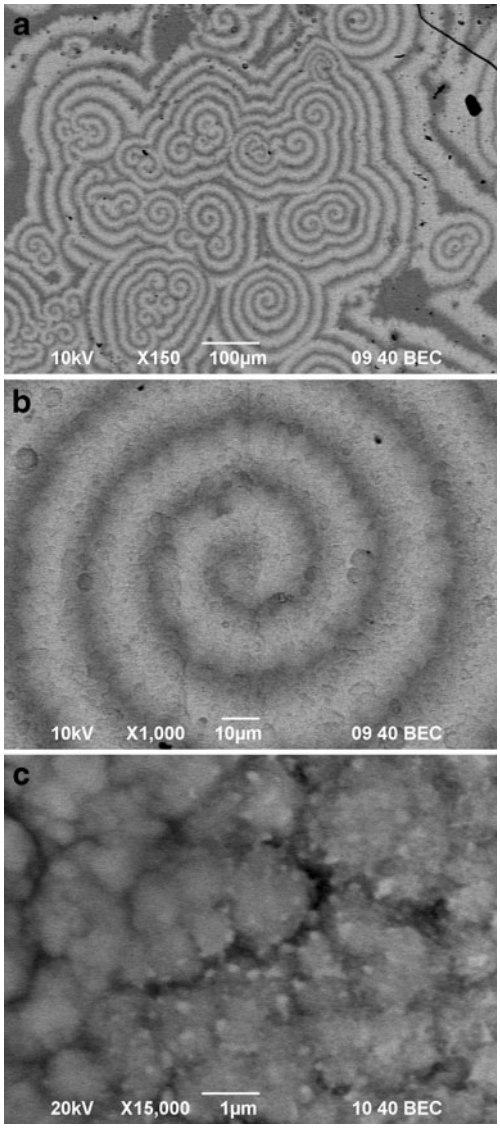

Fig. 5 **a**, **b** SEM images of an In-Co alloy coating, obtained at 1.2 A dm^{-2} from the electrolyte C at different magnification; **c** *light* and *dark zones of the spiral*, shown in **b**

At low current density (0.4 A dm^{-2}, curve 1) except the reflexes of In and $CoIn_3$ phases a small reflex of Cu-In phase is detected. The reflexes of Co (PDF 01-089-7093, hexagonal, with cell parameter a=8.288 Å, c=10.543 Å) appear when the content of the cobalt in the coatings reaches more than 40 wt. %. Some reflexes of copper (substrate) also could be detected (the thickness of the coatings is about 1.5–3 µm). According to the phase diagram [23], and to the fact that the investigated coatings with spatio-temporal structures contain 30–40 wt. % of indium, it could be supposed that one of the phases forming these structures is the $CoIn_3$ phase. To determine the second phase, which cannot be pure indium, according to previous investigations [10], additional X-ray experiments should be performed. The preliminary investigations show, that the spatio-

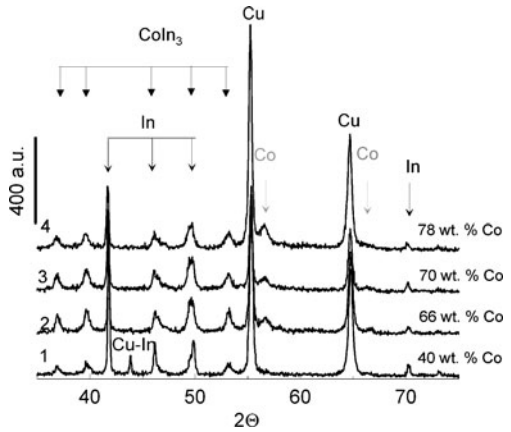

Fig. 6 XRD spectra of the coatings, obtained from the electrolyte A, with current density and time of deposition, 1–0.4 A dm^{-2}, 50 min; 2–0.8 A dm^{-2}, 25 min; 3–1.2 A dm^{-2}, 17 min; 4–1.6 A dm^{-2}, 13 min

temporal structures still exist after several hours heating at 250 °C. This temperature is much higher than the melting temperature of the indium.

At high current densities, semi-bright cobalt-rich coatings are deposited, which are cracked, possibly due to very high internal stress. The stress measurements are presented in Fig. 7, which shows the dependence of the sensor signal in the Stalzer apparatus during deposition. There is not any other known information about the internal stress of electro-deposited indium except that, obtained from the cyanide electrolytes [24]. Typically the stress values of pure indium are very low. The contribution of cobalt to the sign and value of the internal stress of the alloy coatings is stronger than that of indium because the cobalt coatings have a relatively high tensile stress, according to other investigations [25]. The increase of the sensor signal at short deposition times is connected with the increase in the thickness of the coatings and with the effect of cobalt in the alloy

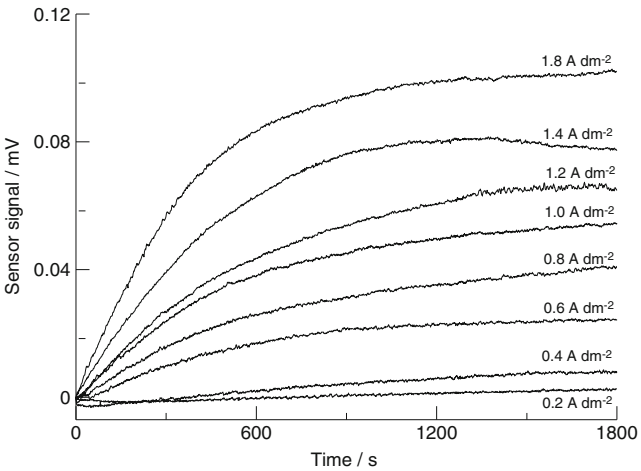

Fig. 7 Changes of the sensor signal with time during IS measurements at coatings, obtained from the electrolyte C

deposit. Depending on the applied current density stress values of about 17 N mm^{-2} could be reached. With further deposition (at longer deposition times), the changes of the sensor signal are not so fast and a plateau is reached, possible due to crack formation in the coatings, which leads to the relaxation of the stress in the coating.

In order to increase the rate of electrodeposition (normally the rate of deposition under applied conditions is about 0.1 μm min^{-1}), the deposition process was performed under favored mass transport conditions, at extremely high velocity of the hydrodynamic flow compared with the flow in the silent electrolyte, due to the natural convection. The experiments were performed in a Jet-cell with current densities between 10 and 50 A dm^{-2}.

The optical images of the electrodes with the obtained coatings from electrolytes A, B and C are shown in Fig. 8. The number of columns corresponds to current densities in the following ways, 1–10, 2–20, 3–30, 4–40 and 5–50 A dm^{-2}. The obtained deposits are light, grey and shiny.

At very high cobalt contents in the coatings deposited in the Jet-cell from electrolyte A, (current densities higher than 30 A dm^{-2}) bad adhesion and cracks in the deposits are observed. The content of the indium in the obtained coatings decreases almost linearly from 98 to 32 wt. % of indium in the three investigated electrolytes (Fig. 9), i.e. the enhanced mass transport favours, as expected, the indium deposition.

Figure 10 shows the relationship between the rate of deposition and current density under the applied high speed deposition conditions. The high speed plating leads to an increase in the rate of deposition almost 10 times in comparison with the conventional electroplating process, which corresponds to literature data on Jet-plating deposition [26–28]. The most effective deposition process was performed in the electrolyte A, but in a smaller current density interval.

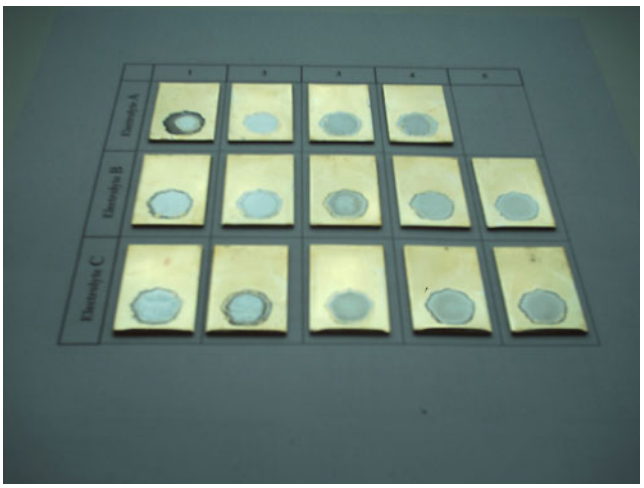

Fig. 8 Optical image of the obtained indium cobalt coatings in the Jet-cell. The number of columns corresponds to current densities in the following way, 1–10, 2–20, 3–30, 4–40 and 5–50 A dm^{-2}

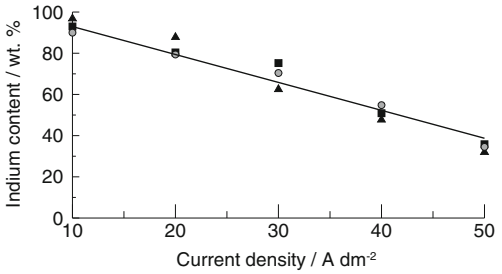

Fig. 9 Content of In in dependence on the current densities in the electrolytes under high-speed plating conditions. *A filled square*, *B filled circle*, *C filled triangle*

Microscopic investigations of the obtained coatings in the Jet-cell show again pattern formation onto the electrode surface (Fig. 11 a–c). The SEM images of the samples, presented in Fig. 11b,c, are presented in Fig. 12. The EDX analysis show an indium content of about 70–75 wt. % in the different areas of the observed structures, which corresponds better to the XRD-data on presented in Fig. 6. The thickness of the sample is approximately 1 μm and the observed structures cover almost the whole surface of the deposits. A big variety of structures, like spirals, waves, targets in different scales could be observed on the surface of the Jet-cell cathode.

Generally patterns were observed when some instability in the electrochemical system appears. The patterns are formed, when the lattice of the basic metal is saturated with the atoms of the alloying metal and the co-deposited excess amount of the later contributes to the formation of new richer in this element phase. Heterogeneous coatings are obtained in this case with chaotically or ordered distribution of the metallic phases presented in the coating.

The hydrodynamic conditions play an important role in the formation of the spatio-temporal structures. Under enhanced mass-transport conditions at high flow rate the structures can be formed at higher current densities possibly corresponding to the same or similar phase composition of the alloy.

The observation of spatio-temporal structures under Jet-plating conditions is a very important step in our studies on

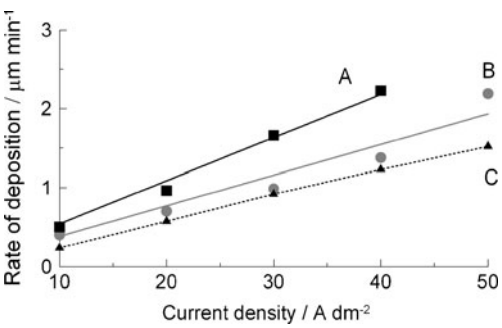

Fig. 10 Rate of deposition of the Co-In alloy depending on the current density at high-speed plating conditions; electrolytes—*A filled square*, *B filled circle*, *C filled triangle*

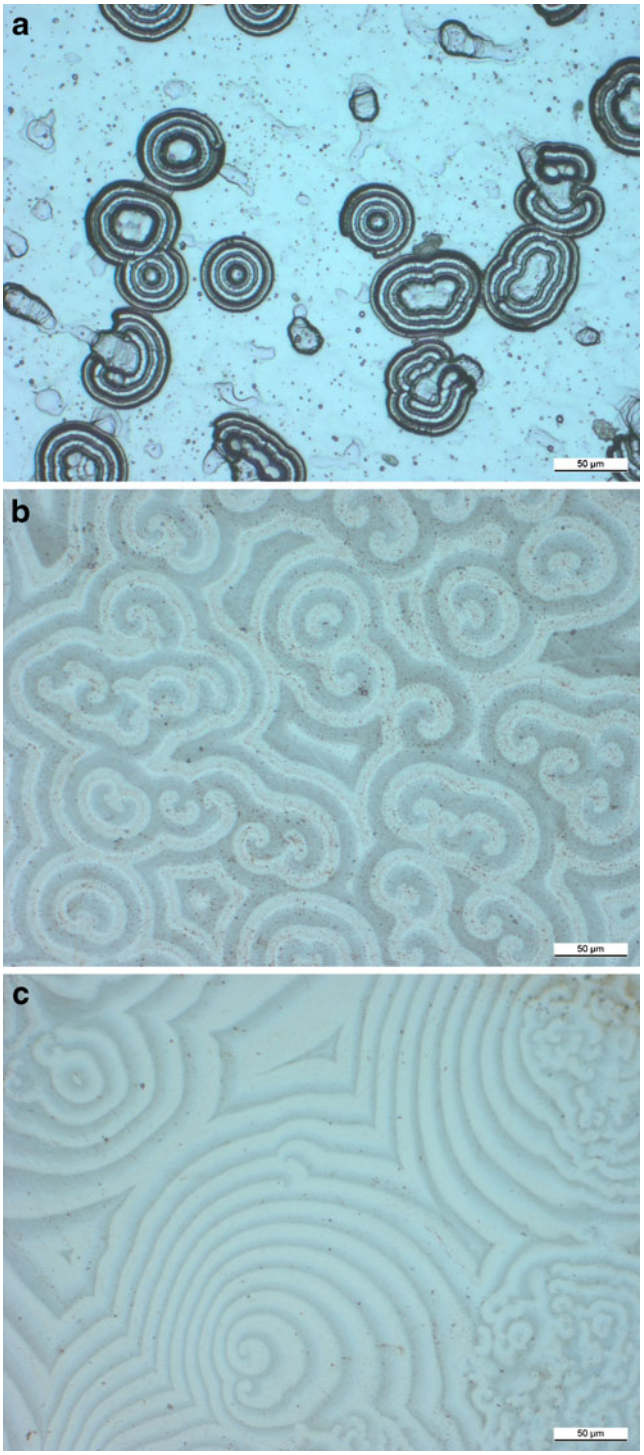

Fig. 11 Optical image of the coatings, obtained in the electrolytes, at current densities and time of deposition as follows: **a** in the electrolyte A—30 A dm^{-2}, 90 s; **b** in the electrolyte B—40 A dm^{-2}, 72 s; **c** in the electrolyte C—50 A dm^{-2}, 60 s

the self-organization phenomena because in all previous investigations similar structures were observed during electrodeposition of alloys in still, non-agitated electrolytes. The assumption that the spatio-temporal structures can be observed

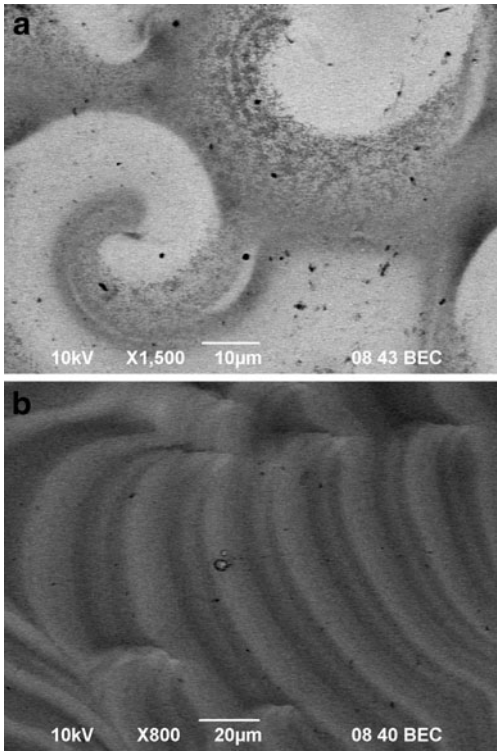

Fig. 12 **a** SEM image of the coating, presented in Fig. 11b. **b** SEM image of the coating, presented in Fig. 11c

under electrolyte agitation at different electrolysis conditions (higher current densities) was confirmed, which opens new possibilities for investigation of the phenomenon under well-controlled hydrodynamic conditions.

Conclusions

1. Indium and cobalt could be successfully deposited from acid citrate electrolytes and deposition of alloys with indium content between 20 and 80 wt. % is possible.
2. At high cobalt content heterogeneous multiphase coatings with spatio-temporal structures can be obtained.
3. The structures are obtained for the first time from silver- and cyanide-free non alkaline stable electrolytes of a relatively simple composition.
4. Spatio-temporal structures could be observed also during electrodeposition under intensive hydrodynamic flow and improved mass transport conditions at high current densities.

Acknowledgements The authors are grateful to the Deutsche Forschungsgemeinschaft (DFG) for the support of the project 436 BUL 113/97/0-4. They express their gratitude to Umicore Galvanotechnik GmbH, Germany for the given possibility to perform high-speed plating experiments in the Jet-cell.

References

1. Dobrovolska Ts, Veleva L, Krastev I, Zielonka A (2005) Composition and structure of silver-indium alloy coatings electrodeposited from cyanide electrolytes. J Electrochem Soc 152:C137–C142
2. Nineva S, Dobrovolska T, Krastev I (2011) Electrodeposition of silver-cobalt coatings. The cyanide-pyrophosphate electrolyte. Bulg Chem Commun 43:96–104
3. Nineva S, Dobrovolska T, Krastev I (2011) Properties of electrodeposited silver-cobalt coatings. J Appl Electrochem 41:1397–1406
4. Dobrovolska T, Krastev I, Jovic BM, Jovic VD, Beck G, Lacnjevac U, Zielonka A (2011) Phase identification in electrodeposited Ag-Cd alloys by anodic linear sweep voltammetry and X-ray diffraction techniques. Electrochim Acta 56:4344–4350
5. Kristev I, Nikolova M (1986) Structural effects during the electrodeposition of silver-antimony alloys from ferrocyanide-thiocyanate electrolytes. J Appl Electrochem 16:875–878
6. Krastev I, Valkova T, Zielonka A (2004) Structure and properties of electrodeposited silver-bismuth alloys. J Appl Electrochem 34:79–85
7. Valkova T, Krastev I, Zielonka A (2010) Influence of the D(+)-glucose on the electrochemical deposition of Ag-Bi alloy from a cyanide electrolyte. Bulg Chem Commun 42:317–322
8. Hrussanova A, Krastev I (2009) Electrodeposition of silver-tin alloys from pyrophosphate-cyanide electrolytes. J Appl Electrochem 39:989–994
9. Ts D, Krastev I, Zielonka A (2005) Effect of the electrolyte composition on In and Ag-In alloy electrodeposition from cyanide electrolytes. J Appl Electrochem 35:1245–1251
10. Krastev I, Ts D (2010) Self-organized structure formation and phase identification in electrodeposited silver-cadmium, silver-indium and cobalt-indium alloys. J Eng Process Manag 2:99–105
11. Gabay AM, Hadjipanayis GC (2010) Phases and phase equilibria in cobalt-rich Pr-Co-In alloys for permanent magnets. J Alloys Compd 500:161–166
12. Sadana YN, Keskinen AE, Guindon M (1975) Electrodeposition of alloys III Electrodeposition and X-ray structure of cobalt-indium alloys (initial studies). Electrodeposition Surf Treat 3:149–157
13. Stalzer M (1964) Geräte für Spannungsmessungen an galvanisch abgeschiedenen Schichten und Beschreibung eines neuentwickelten selbstkompensierenden und registrierenden Gerätes. Metalloberfläche 263–267
14. Wingenfeld P (2004) Selective high-speed plating of noble metals in reel-to-reel plants—Part 6. Galvanotechnik 95:879–884
15. Speight JG (2005) Lange's handbook of chemistry. McGraw-Hill, New York
16. Alderighi L, Gans P, Ienco A, Peters D, Sabatini A, Vacca A (1999) Hyperquad smulation and speciation (HySS): a utility program for the investigation of equilibria involving soluble and partially soluble species. Coord Chem Rev 184:311–318
17. Maki N, Tanaka N (1975) Cobalt, chapter III. In: Bard JA (ed) Encyclopedia of electrochemisrty of the elements. Marcel Dekker Inc, New York, pp 43–210
18. Losev VV, Molodov AI (1976) Indium, chapter I. In: Bard JA (ed) Encyclopedia of electrochemisrty of the elements. Marcel Dekker Inc, New York, pp 1–32
19. Frier M, Ellis J, Aslam M (1996) Stability of radiopharmaceuticals during administration to the intensive care patient. J Clin Pharm Ther 21:149–153
20. Mohammad B, Ure AM, Littlejohn D (1993) On-line preconcentration of aluminium, gallium and indium with quinolin-8-ol for determination by atomic absorption spectrometry. J Anal At Spectrom 8:325–331
21. Wood SA, Samson IM (2006) The aqueous geochemistry of gallium, germanium, indium and scandium. Ore Geol Rev 28:57–102
22. Lacroix S (1949) E´tude de quelques complexes et compose´ speu solubles des ions Al^{3+}, Ga^{3+}, In^{3+}. Ann Chim 4:5–83
23. Liakishev NP (1997) Diagrammy sostojanija dvojnyh metallicheskih sistem. Mashinostroenie, Moskva, pp 37–38
24. Krastev I, Dobrovolska T, Kowalik R, Zabinski P, Zielonka A (2009) Properties of silver-indium alloys electrodeposited from cyanide electrolytes. Electrochim Acta 54:2515–2521
25. Sotirova G, Sarnev S, Armyanov S (1989) Evolution of the included hydrogen, internal stress, microharness and microstructure of electrodeposited cobalt. Electrochim Acta 34:1237–1242
26. Raub CJ (1990) Jet plating. Laboratory simulation and control. Trans Inst Met Finish 68:115–117
27. De Vogelaere M, Sommer V, Springborn H, Michelsen-Mohammadein U (2001) High-speed plating for electronic applications. Electrochim Acta 47:109–116
28. Qiao G, Jing T, Wang N, Gao Y, Zhao X, Zhou J, Wang W (2006) Effect of current density on microstructure and properties of bulk nanocrystalline Ni-Co alloys prepared by JED. J Electrochem Soc 153:C305–C308